THE JOURNAL OF PHYSICAL CHEMISTRY A

Article

pubs.acs.org/JPCA

Vibrational Dynamics of the $CH_4 \cdot F^-$ Complex

Robert Wodraszka,[†] Juliana Palma,[†] and Uwe Manthe*

Theoretische Chemie, Fakultät für Chemie, Universität Bielefeld, Universitätsstrasse 25, D-33615 Bielefeld, Germany

ABSTRACT: Motivated by recent photodetachment experiments studying resonance structures in the transition-state region of the $F + CH_4 \rightarrow HF + CH_3$ reaction, the vibrational dynamics of the precursor complex $CH_4 \cdot F^-$ is investigated. Delocalized vibrational eigenstates of $CH_4 \cdot F^-$ are computed in full dimensionality employing the multiconfigurational time-dependent Hartree (MCTDH) approach and a recently developed iterative diagonalization approach for general multiwell systems. Different types of stereographic coordinates are used, and a corresponding general *N*-body kinetic energy operator is given. The calculated tunneling splittings of the ground and the lower vibrational excited states of the $CH_4 \cdot F^-$ complex do not significantly exceed 1 cm^{-1}. Comparing the converged MCTDH results for localized vibrational excitations with existing results obtained by normal-mode-based (truncated) vibrational configuration interaction calculations, significantly lower frequencies are found for excitations in the intermolecular modes.

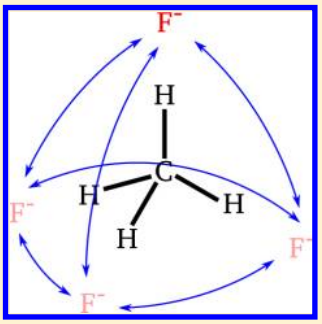

1. INTRODUCTION

Fundamental studies of elementary chemical reactions increasingly focus on polyatomic systems consisting of more than three or four atoms. The increased complexity of these polyatomic reactions offers many interesting new questions and challenges. Reactions of methane with different atoms such as F, Cl, H, or O provide prototypical examples that are extensively studied by experiment and theory.[1−23] While these studies typically describe the chemical reaction as a reactive scattering process, recently, the $F + CH_4 \rightarrow HF + CH_3$ system has also been investigated employing a transition-state spectroscopy approach.[24,25] In these experiments, photodetachment of the anionic $CH_4 \cdot F^-$ complex generates the neutral $CH_4 \cdot F$ system at an initial geometry close to the transition state. The subsequent reaction then yields $F + CH_4$ as well as $HF + CH_3$ products.

The low-resolution photodetachment spectrum of $CH_4 \cdot F^-$ shows two broad peaks. The first peak shows a much higher intensity, and the difference in electron binding energy between the peaks is about 1300−1400 cm^{-1}. This spectrum has very recently also been studied theoretically by full-dimensional wave packet dynamics calculations[26] employing the multiconfigurational time-dependent Hartree (MCTDH) approach[27,28] and potential energy surfaces (PESs) developed by Bowman and co-workers.[6,29] Here, a localized vibrational state of $CH_4 \cdot F^-$ has been employed as the initial wave packet, which was vertically excited to the PES of the neutral complex by the photodetachment process. The calculations were restricted to propagation times of about 100 fs and correspondingly could not provide an energy resolution better than 100 cm^{-1} . Experimentally, Neumark and co-workers could also measure a high-resolution photodetachment spectrum that shows interesting resonance structures superimposed on the first peak.[25] The energy spacings seen there are in the 10−30 cm^{-1} region and have not yet been addressed by theoretical investigations.

Considering the high-resolution photodetachment experiments, a fundamental question regarding the vibrational structure of $CH_4 \cdot F^-$ arises. The PES of $CH_4 \cdot F^-$ shows four symmetry-equivalent minima.[29] In principle, the vibrational ground state of $CH_4 \cdot F^-$ would thus be delocalized. Whether a localized model can also provide a valid description depends on the tunneling splitting of the delocalized eigenstates. These splittings are mainly determined by the height and width of the barrier separating the minima and by the mass of the tunneling atoms. In $CH_4 \cdot F^-$, the complex can change from one minimum to another by only rotating the methane relative to the fluorine, a motion that includes only movement of hydrogen atoms. Furthermore, the height of the barriers separating the minima is only about 4 kcal/mol. It should be noted that this value is comparable to the barrier height found in malonaldehyde, a benchmark proton-transfer system showing a tunneling splitting of about 20 cm^{-1}. The present work will investigate whether a sizable tunneling splitting can also be found in the $CH_4 \cdot F^-$ complex.

Czakó et al.[29] already investigated the vibrational states of the $CH_4 \cdot F^-$ complex. However, they employed normal coordinates and a (single-reference) vibrational configuration interaction (VCI)[30,31] scheme. By construction, this approach enforces localization of the vibrational states of $CH_4 \cdot F^-$ in a single potential well. Thus, it cannot provide information concerning tunneling splittings.

The accurate calculation of delocalized vibrational eigenstates in polyatomic systems is a challenging task. There are only a few examples of systems consisting of six or more atoms that have been studied in full dimensionality, the molecular hydrogen trimer $(H_2)_3$,[32] CH_5^+,[33] the protonated water dimer

Special Issue: Jörn Manz Festschrift

Received: May 30, 2012
Revised: June 25, 2012

   dx.doi.org/10.1021/jp3052642 | *J. Phys. Chem. A* XXXX, XXX, XXX−XXX

$H_5O_2^+$,[34−38] or malonaldehyde.[39−45] These calculations employed very elaborate discrete variable representation (DVR) schemes,[32,33] diffusion Monte Carlo based approaches,[39,40,42] or the MCTDH approach.[34−39,41,43−45] In analogy to the investigation of the symmetric double-well system malonaldehyde, the present work will use the MCTDH approach to study the vibrational eigenstates of $CH_4{\cdot}F^-$.

The MCTDH calculations for malonaldehyde utilized the symmetry of the double-well structure of the PES to reduce the numerical effort. However, the schemes employed, which are described in detail in ref 41, are restricted to specific symmetries and cannot be employed for more complex multiwell systems. In particular, they cannot be applied to the T_d-symmetric four-well PES of the $CH_4{\cdot}F^-$ complex. Therefore, very recently, a more general scheme was proposed that allows one to utilize more general symmetries and multiwell structures in MCTDH calculations of delocalized vibrational eigenstates.[46] Studying $CH_4{\cdot}F^-$, the present work will present the first application of this approach to a real molecular system.

To describe the large-amplitude motion in the intermolecular coordinates of $CH_4{\cdot}F^-$, the present work employs curvilinear coordinates. While standard Jacobi and Radau constructions are used to define the underlying orthogonal vectors, the parametrization of these vectors employs the recently introduced stereographic coordinates.[47] Originally, the stereographic coordinates were introduced to avoid relevant singularities in the kinetic energy operator describing the H + CH_4 → H_2 + CH_3 reaction.[21,22,47] In the present work, the definition of the stereographic coordinates is extended. A corresponding general *N*-body kinetic energy operator is derived and applied to the study of the vibrational states of $CH_4{\cdot}F^-$.

The article is organized as follows. The theory section (section 2) starts with a description of the stereographic coordinates and the corresponding general *N*-body kinetic energy operator. Then, the MCTDH approach is briefly reviewed, and the multiwell iterative diagonalization approach is described. Section 3 focuses on the details of the $CH_4{\cdot}F^-$ system. The coordinate system, the PES, symmetry considerations, and the wave function representation are discussed. Then, the results are presented and discussed in section 4. Concluding remarks complete this article.

2. THEORY

A. Stereographic Coordinates and an *N*-Body Kinetic Energy Operator. The present work employs a generic *N*-body kinetic energy operator that uses stereographic coordinates to parametrize the vectors not involved in the definition of the body-fixed frame. Stereographic coordinates parametrize a vector **r** by its length r and the coordinates s,t, which determine its orientation with respect to a reference frame. Reference 47 introduced stereographic coordinates with a projection that employs the south pole of the unit sphere to construct the orientational coordinates s,t (see Figure 1a). The s,t coordinates equal the x,y coordinates of the intersection point of the equatorial plane ($z = 0$) and the line connecting the south pole and the point on the unit sphere. Thus, $s^2 + t^2 \leq 1$ holds for the points of the northern hemisphere, while the points of the southern hemisphere yield $s^2 + t^2 > 1$. The north pole has the coordinates $s = t = 0$, whereas the south pole cannot be represented. The formulas connecting spherical polar coordinates (r,ϑ,φ) and Cartesian coordinates (x,y,z) with stereographic ones read[47]

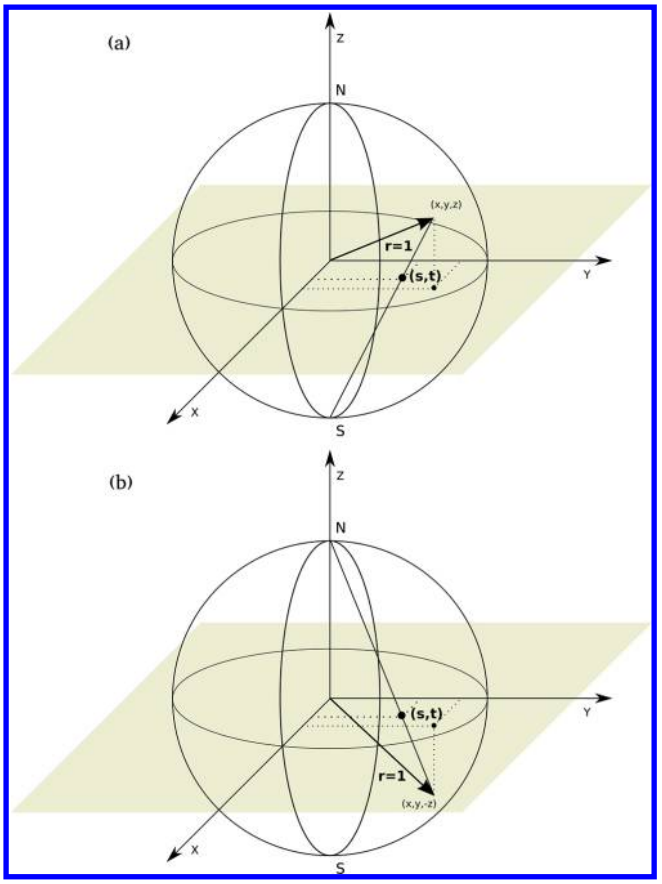

Figure 1. Stereographic coordinates constructed via a projection from the south pole or the north pole of the unit sphere are displayed in panels (a) and (b), respectively.

$$s = \tan\left(\frac{\vartheta}{2}\right)\cos\varphi$$
$$t = \tan\left(\frac{\vartheta}{2}\right)\sin\varphi \quad (1)$$

and

$$x = 2r\frac{s}{1 + s^2 + t^2}$$
$$y = 2r\frac{t}{1 + s^2 + t^2}$$
$$z = r\frac{1 - s^2 - t^2}{1 + s^2 + t^2} \quad (2)$$

Choosing ordinary spherical polar coordinates to derive the kinetic energy operator, singularities appear at $\vartheta = 0$ and π, that is, for points lying on the whole z-axis. Utilizing the stereographic coordinates defined above, only the negative half of the z-axis cannot be represented. Consequently, these coordinates yield a kinetic energy operator with no singularities in the terms describing the nonembedding vectors. However, the negative z-axis is not accessible by the dynamics of the corresponding particle within this description.

In contrast to ref 47, this work also considers particles whose motion does not exclude the negative z-axis but the positive z-axis. To allow for a correct description of their dynamics, the corresponding stereographic coordinates constructed via a projection from the north pole are introduced (see Figure 1b).

dx.doi.org/10.1021/jp3052642 | J. Phys. Chem. A XXXX, XXX, XXX−XXX

Here, the line that intersects the equatorial plane connects the north pole with the point on the unit sphere. The points of the southern hemisphere are mapped to the region inside of the unit circle lying in the equatorial plane, while the points of the northern hemisphere are mapped outside of this circle. The south pole is located at $s = t = 0$, and the north pole cannot be represented. The formulas corresponding to the ones given above now read

$$s = \cot\left(\frac{\vartheta}{2}\right)\cos\varphi$$
$$t = \cot\left(\frac{\vartheta}{2}\right)\sin\varphi \tag{3}$$

and

$$x = 2r\frac{s}{1+s^2+t^2}$$
$$y = 2r\frac{t}{1+s^2+t^2}$$
$$z = r\frac{s^2+t^2-1}{1+s^2+t^2} \tag{4}$$

Please note that eqs 2 and 4 differ only in the signs of the z coordinates. This can also be understood by inspecting Figure 1. There, the points on the sphere are chosen to be related by a reflection through the equatorial plane, that is, they differ only in the signs of their z coordinates.

Within the construction corresponding to Figure 1b, only the positive half of the z-axis cannot be represented. Thus, by employing both sets of stereographic coordinates (projection from the south pole and from the north pole) simultaneously for the derivation of the kinetic energy operator, each nonembedding vector can be parametrized according to the dynamically relevant region of the corresponding particle. This avoids the appearance of singularities inherent when utilizing ordinary spherical polar coordinates.

In the following, a generic kinetic energy operator corresponding to stereographic coordinates is derived for a molecular system that consists of N nuclei. After separation of the overall translational motion, the system is described by $N-1$ vectors. A right-handed body-fixed frame is defined by attaching the z-axis along the first vector $\mathbf{r}_1$ and constraining the second vector $\mathbf{r}_2$ to lie in the positive half of the xz-plane. To describe these two embedding vectors, the internal coordinates are chosen as r_1,r_2, which denote the mass-weighted lengths, and θ, which denotes the angle enclosed by the two vectors. Further assuming that the $N-1$ vectors employed are orthogonal (e.g., a mixture of Jacobi and Radau vectors), the kinetic energy operator with respect to the body-fixed frame reads (see, e.g., ref 48 for a detailed discussion)

$$\hat{T}_{(N-1)\mathrm{V}} = \hat{T}_{2\mathrm{V}}\left(r_1, r_2, \theta, \hat{\mathbf{J}} - \sum_{i=3}^{N-1}\hat{\mathbf{L}}_i\right) - \sum_{i=3}^{N-1}\frac{1}{2}\Delta_{\mathbf{r}_i} \tag{5}$$

Here, the $\{\mathbf{r}_i, i \geq 3\}$ are the mass-weighted vectors not used to define the reference frame and $\Delta_{\mathbf{r}_i}$ represents the corresponding Laplace operator. $\hat{T}_{2\mathrm{V}}$ is the kinetic energy operator for a triatomic system (or equivalently for a two-vector model).[49] It depends on the aforementioned three internal coordinates r_1,r_2,θ and on the operator $\hat{\mathbf{J}} - \sum_{i=3}^{N-1}\hat{\mathbf{L}}_i$. Here, $\hat{\mathbf{J}}$ denotes the angular momentum operator associated with the overall rotation of the N-atomic system, and $\{\hat{\mathbf{L}}_i, i \geq 3\}$ are the angular momentum operators associated with the nonembedding vectors. The explicit form of $\hat{T}_{2\mathrm{V}}$ reads

$$\begin{aligned}\hat{T}_{2\mathrm{V}}(r_1, r_2, \theta, \hat{\mathbf{J}}_{2\mathrm{V}}) = &-\frac{1}{2}\frac{\partial^2}{\partial r_1^2} - \frac{1}{2}\frac{\partial^2}{\partial r_2^2} - \frac{1}{2}\left(\frac{1}{r_1^2}+\frac{1}{r_2^2}\right)\\ &\frac{1}{\sqrt{\sin\theta}}\frac{\partial}{\partial\theta}\sin\theta\frac{\partial}{\partial\theta}\frac{1}{\sqrt{\sin\theta}}\\ &+\frac{1}{2r_1^2}(\hat{J}_{2\mathrm{V},x}^2+\hat{J}_{2\mathrm{V},y}^2)\\ &+\frac{1}{2}\left(\frac{\cot^2\theta}{r_1^2}+\frac{\csc^2\theta}{r_2^2}\right)\hat{J}_{2\mathrm{V},z}^2\\ &+\frac{\cot\theta}{2r_1^2}(\hat{J}_{2\mathrm{V},x}\hat{J}_{2\mathrm{V},z}+\hat{J}_{2\mathrm{V},z}\hat{J}_{2\mathrm{V},x})\\ &+\frac{\mathrm{i}}{r_1^2}\frac{\partial}{\partial\theta}\hat{J}_{2\mathrm{V},y}\end{aligned} \tag{6}$$

$\hat{\mathbf{J}}_{2\mathrm{V}}$ is the angular momentum operator associated with the overall rotation of the triatomic system. It should be noted that the volume element $v = r_1^2 r_2^2 \sin\theta$ is incorporated in the operator given above (i.e., $\hat{T}_{2\mathrm{V}} \rightarrow v^{1/2}T_{2\mathrm{V}}v^{-1/2}$). Moreover, angular momentum operators $\hat{J}_{2\mathrm{V},\alpha}$ that obey the anomalous commutation relations[50] are used in contrast to ref 49. Utilizing this explicit form of $\hat{T}_{2\mathrm{V}}$ in the expression of eq 5, the kinetic energy operator for the $N-1$ vector model

$$\begin{aligned}\hat{T}_{(N-1)\mathrm{V}} = &-\frac{1}{2}\frac{\partial^2}{\partial r_1^2} - \frac{1}{2}\frac{\partial^2}{\partial r_2^2} - \frac{1}{2}\left(\frac{1}{r_1^2}+\frac{1}{r_2^2}\right)\\ &\frac{1}{\sqrt{\sin\theta}}\frac{\partial}{\partial\theta}\sin\theta\frac{\partial}{\partial\theta}\frac{1}{\sqrt{\sin\theta}}\\ &-\sum_{i=3}^{N-1}\left(\frac{1}{2}\frac{\partial^2}{\partial r_i^2}-\frac{\hat{L}_i^{\,2}}{2r_i^2}\right)\\ &+\frac{1}{2r_1^2}\left\{\hat{J}_x^2+\hat{J}_y^2-2\left(\hat{J}_x\sum_{i=3}^{N-1}\hat{L}_{i,x}+\hat{J}_y\sum_{i=3}^{N-1}\hat{L}_{i,y}\right)\right.\\ &\left.+\sum_{i,j=3}^{N-1}(\hat{L}_{i,x}\hat{L}_{j,x}+\hat{L}_{i,y}\hat{L}_{j,y})\right\}\\ &+\frac{1}{2}\left(\frac{\cot^2\theta}{r_1^2}+\frac{\csc^2\theta}{r_2^2}\right)\left(\hat{J}_z^2-2\hat{J}_z\sum_{i=3}^{N-1}\hat{L}_{i,z}\right.\\ &\left.+\sum_{i,j=3}^{N-1}\hat{L}_{i,z}\hat{L}_{j,z}\right)\\ &+\frac{\cot\theta}{2r_1^2}\left\{\hat{J}_x\hat{J}_z+\hat{J}_z\hat{J}_x-2\left(\hat{J}_x\sum_{i=3}^{N-1}\hat{L}_{i,z}+\hat{J}_z\sum_{i=3}^{N-1}\hat{L}_{i,x}\right)\right.\\ &\left.+\sum_{i,j=3}^{N-1}\left(\hat{L}_{i,x}\hat{L}_{j,z}+\hat{L}_{i,z}\hat{L}_{j,x}\right)\right\}+\frac{\mathrm{i}}{r_1^2}\frac{\partial}{\partial\theta}\left(\hat{J}_y-\sum_{i=3}^{N-1}\hat{L}_{i,y}\right)\end{aligned} \tag{7}$$

is obtained. To derive an explicit form of the kinetic energy operator, the angular momentum operators $\hat{\mathbf{L}}_i$ have to be expressed in the stereographic coordinates s,t introduced above. The corresponding equation reads

dx.doi.org/10.1021/jp3052642 | J. Phys. Chem. A XXXX, XXX, XXX−XXX

$$\hat{\mathbf{L}} = \frac{1}{2\mathrm{i}}\left[\begin{pmatrix} -2st\cdot\sigma \\ (1+s^2-t^2)\cdot\sigma \\ -2t \end{pmatrix}\frac{\partial}{\partial s} - \begin{pmatrix} (1-s^2+t^2)\cdot\sigma \\ -2st\cdot\sigma \\ -2s \end{pmatrix}\frac{\partial}{\partial t} + \begin{pmatrix} -2t\cdot\sigma \\ 2s\cdot\sigma \\ 0 \end{pmatrix}\right] \tag{8}$$

Again, the volume element $v = 4r^2/(1+s^2+t^2)^2$ is incorporated in the operator equation above.[47] σ determines if the stereographic projection coordinates are constructed using the south pole ($\sigma = 1$) or the north pole ($\sigma = -1$) projection. Thus, the corresponding angular momentum operators differ only in the signs of the respective x and y components. The squared form $\hat{L}^2$ is equal for both constructions and reads

$$\hat{L}^2 = -\frac{1}{4}(1+s^2+t^2)\left(\frac{\partial^2}{\partial s^2} + \frac{\partial^2}{\partial t^2}\right)(1+s^2+t^2) \tag{9}$$

In eq 7, each $\hat{\mathbf{L}}_i$ with $i \geq 3$ can now be described utilizing one of the two types of stereographic coordinates presented above. This choice should be made in a way to provide an efficient description of the dynamically relevant regions of the respective particle considered.

B. MCTDH Approach. The MCTDH approach[27,28,51] provides an efficient method for the accurate simulation of multidimensional quantum dynamics. In the present work, the state-averaged MCTDH scheme[52] is used. The wave function ansatz reads

$$\Psi_p(q_1^1, q_2^1, ..., q_d^1, t) = \sum_{j_1=1}^{n_1} ... \sum_{j_d=1}^{n_d} A^1_{j_1,...,j_d,p}(t)\cdot\phi^{1;1}_{j_1}(q_1^1, t)\cdot ...\cdot\phi^{1;d}_{j_d}(q_d^1, t) \qquad p = 1, ..., P \tag{10}$$

A set of P wave packets Ψ_p is represented within a common basis of time-dependent single-particle functions (SPFs) $\phi^{1;\kappa}_{j_i}$ using the time-dependent expansion coefficients $A^1_{j_1,...,j_d,m}$. In the original MCTDH scheme,[27,28] each $\phi^{1;\kappa}_{j_i}$ is itself expanded in an underlying time-independent basis or equivalently on a grid utilizing a discrete variable representation (DVR)[53−55] or a fast Fourier transform (FFT) scheme[56]

$$\phi^{1;\kappa}_{j_\kappa}(q^1_\kappa, t) = \sum_{i=1}^{N_\kappa} A^{2;\kappa}_{j_\kappa;i}(t)\cdot\chi^{2;\kappa}_i(q^1_\kappa) \tag{11}$$

This scheme corresponds to a two-layer representation, where the superscripts 1 and 2 denote the upper and lower layers, respectively. In the multilayer extension of the MCTDH approach,[57,58] the $\phi^{1;\kappa}_{j_\kappa}$ can be multidimensional functions which themselves are recursively represented by other sets of SPFs

$$\begin{aligned}\phi^{1;\kappa}_m(q^1_\kappa, t) &= \phi^{1;\kappa}_m(q_1^{2;\kappa}, ..., q_{d_\kappa}^{2;\kappa}, t) \\ &= \sum_{j_1=1}^{n_{\kappa,1}} ... \sum_{j_{d_\kappa}=1}^{n_{\kappa,d_\kappa}} A^{2;\kappa}_{m;j_1,...,j_{d_\kappa}}(t)\cdot\phi^{2;\kappa,1}_{j_1}(q_1^{2;\kappa}, t)\cdot ...\cdot\phi^{2;\kappa,d_\kappa}_{j_{d_\kappa}}(q_{d_\kappa}^{2;\kappa}, t)\end{aligned} \tag{12}$$

Here, $\phi^{1;\kappa}_m$ depends on the multidimensional coordinate q^1_κ, which combines a set of coordinates $q_1^{2;\kappa}$, ..., $q_{d_\kappa}^{2;\kappa}$. This type of representation can be recursively repeated for the functions $\phi^{2;\kappa,i}_{j_i}$, resulting in a tree-like scheme, until it is terminated by a bottom layer of time-independent functions, as shown in eq 11.

For the integration of the MCTDH equations of motion, specially adapted propagation schemes can be utilized.[59,60] Specifically, the present work employs the CMF2 scheme of ref 60. The evaluation of potential energy matrix elements appearing in the equations of motion is performed via the correlation discrete variable representation (CDVR).[58,61−63]

C. Multiwell Iterative Diagonalization. The MCTDH approach can be employed to calculate eigenstates of the Hamiltonian $\hat{H}$. Several methods have been developed for this purpose, for example, the iterative diagonalization of the $\exp(-\beta\hat{H})$ operator[64] or the improved relaxation approach.[65] Within the state-averaged MCTDH approach used in the present work, the block relaxation scheme[52] that employs subspace iteration can be utilized.

For the treatment of systems with a multiwelled PES (like the presently investigated $CH_4{\cdot}F^-$ complex), a multiwell iterative diagonalization procedure has recently been presented.[46] Its key idea is to construct a basis of states that are dominantly localized in each well of the potential surface. Considering a system with W wells in the potential, P state-averaged MCTDH wave functions are employed in each well in each step of the iteration procedure. Initial seed vectors $\psi^{(0)}_{wp}$ provide a starting point that induces the localization; each initial wave function $\psi^{(0)}_{wp}$ is well-localized in well w. Then, further sets of (localized) wave functions $\psi^{(n)}_{wp}$ are generated using a block Lanczos-type iteration sequence. The corresponding recursion relations used within this work read

$$\tilde{\psi}^{(n)}_{wp} = \hat{A}\psi^{(n-1)}_{wp} - \sum_{i=0}^{n-1}\sum_{v=1}^{W}\sum_{q=1}^{P}\alpha^{(i)}_{vq}\hat{P}^{(n)}_w\psi^{(i)}_{vq} \tag{13}$$

$$\psi^{(n)}_{wp} = C^{(n)}_{wp}(\tilde{\psi}^{(n)}_{wp} - \sum_{q=0}^{p-1}\psi^{(n)}_{wq}\langle\psi^{(n)}_{wq}|\tilde{\psi}^{(n)}_{wp}\rangle) \tag{14}$$

Here, $\psi^{(n)}_{wp}$ denotes the pth wave packet dominantly localized in well w, which has been generated in the nth iteration step. The operator $\hat{A}$ is chosen as $\exp(-\mathrm{i}\hat{H}t)\exp(-\beta\hat{H})$. $\hat{P}^{(n)}_w$ is a projector onto the SPF basis of $\hat{A}\psi^{(n-1)}_{wp}$. The $\alpha^{(i)}_{vq}$ are given by the set of linear equations

$$\langle\hat{P}^{(n)}_w\psi^{(j)}_{ur}|\hat{A}\psi^{(n-1)}_{wp}\rangle = \sum_{i=0}^{n-1}\sum_{v=1}^{W}\sum_{q=1}^{P}\alpha^{(i)}_{vq}\langle\hat{P}^{(n)}_w\psi^{(j)}_{ur}|\hat{P}^{(n)}_w\psi^{(i)}_{vq}\rangle$$
$$j = 0, ..., n-1;\ u = 1, ..., W;\ r = 1, ..., P \tag{15}$$

The states $\psi^{(n)}_{wp}$ then serve as a basis for the diagonalization of the Hamiltonian $\hat{H}$ (or a bijective function of it). In this work, eigenstates and eigenenergies of the Hamiltonian $\hat{H}$ are obtained by diagonalizing $\exp(-\mathrm{i}\hat{H}t)$ in the basis of $\exp(-\beta\hat{H})\psi^{(j)}_{wp}$. To this end, the generalized eigenvalue problem

$$\sum_{l=0}^{n-1}\sum_{v=1}^{W}\sum_{q=1}^{P}\langle e^{-\beta\hat{H}}\psi^{(j)}_{wp}|e^{-\mathrm{i}\hat{H}t}|e^{-\beta\hat{H}}\psi^{(l)}_{vq}\rangle c^{(l)}_{vq,m} = \sum_{l=0}^{n-1}\sum_{v=1}^{W}\sum_{q=1}^{P}\epsilon_m\langle e^{-\beta\hat{H}}\psi^{(l)}_{wp}|e^{-\beta\hat{H}}\psi^{(l)}_{vq}\rangle c^{(l)}_{vq,m} \tag{16}$$

dx.doi.org/10.1021/jp3052642 | J. Phys. Chem. A XXXX, XXX, XXX−XXX

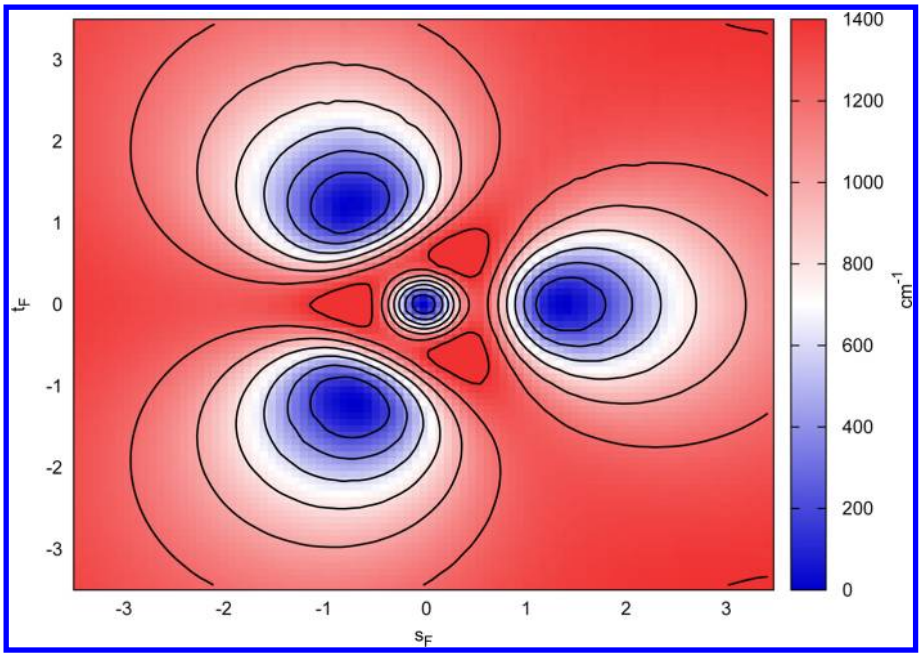

Figure 2. Contour plot of the $CH_4 \cdot F^-$ PES with respect to the coordinates s_F,t_F.

is solved. Here, the $c_{vq,m}^{(l)}$ denote the eigenvector components and ϵ_m the eigenvalues. The eigenvalues ϵ determine the eigenenergy E via $\epsilon = e^{-iEt}$.

In ref 46, also an alternative scheme that employs explicit interwell orthogonalization of the $\hat{A}\psi_{wp}^{(n-1)}$ in the recursion relations was introduced and discussed. However, the system studied in the present work shows only weak coupling between the wave functions localized in the different wells (vide infra). Thus, the use of this more involved scheme would not offer any advantage in the present context.

The key idea of constructing localized functions on multiwelled potential surfaces suggests to interpret vibrational states localized in well w as a useful zeroth-order basis and the interwell coupling as a perturbation. These localized vibrational states can also be obtained within the present approach by solving the generalized eigenvalue problem of eq 16 utilizing the basis of the $\exp(-\beta\hat{H})\psi_{wp}^{(j)}$ for a single value of the well index w only

$$\sum_{l=0}^{n-1}\sum_{q=1}^{P}\langle e^{-\beta\hat{H}}\psi_{wp}^{(j)}|e^{-i\hat{H}t}|e^{-\beta\hat{H}}\psi_{wq}^{(l)}\rangle\tilde{c}_{wq,m}^{(l)} = \sum_{l=0}^{n-1}\sum_{q=1}^{P}\tilde{\epsilon}_{w,m}\langle e^{-\beta\hat{H}}\psi_{wp}^{(j)}|e^{-\beta\hat{H}}\psi_{wq}^{(l)}\rangle\tilde{c}_{wq,m}^{(l)} \quad (17)$$

Thus, the mth local state in well w, which is denoted by $\psi_{w,m}^{(lok)}$ and corresponds to the eigenvalue $\tilde{\epsilon}_{w,m}$, reads

$$\psi_{w,m}^{(lok)} = \sum_{l=0}^{n-1}\sum_{q=1}^{P}\tilde{c}_{wq,m}^{(l)}e^{-\beta\hat{H}}\psi_{wq}^{(l)} \quad (18)$$

Local states defined in this way correspond to localized approximate eigenstates in the well w. In the limit of wells separated by infinitely high barriers, the $\psi_{w,m}^{(lok)}$ would be the exact eigenstates.

It should be noted that the multiwell iterative diagonalization scheme converges the vibrational energy levels from bottom to top, that is, all lower-energy states have to be reasonably well converged before higher-energy states can be reliably obtained.

3. SYSTEM

A. Coordinate System. The coordinate system employed for the description of the $CH_4 \cdot F^-$ complex is based on a mixed Radau–Jacobi construction. After separation of the translational motion of the whole system, four Radau vectors that connect the canonical point with each of the four hydrogens are used to describe the CH_4. A Jacobi vector that connects the center of mass of CH_4 with F^- is used to describe the relative position of the fluorine. Two Radau vectors define the body-fixed frame and are described by the internal coordinates r_1,r_2, and θ. The remaining two Radau vectors are parametrized by the stereographic coordinates r_3,s_3,t_3 and r_4,s_4,t_4. Here, a projection employing the north pole (see Figure 1b) is used because the dynamics of the corresponding hydrogen atoms will take place dominantly in the southern hemisphere. The Jacobi vector is parametrized by the stereographic coordinates r_F,s_F,t_F corresponding to the projection employing the south pole (see Figure 1a).

Considering the tetrahedral equilibrium structure of the methane molecule in the reference frame chosen, one hydrogen atom lies on the positive z-axis, while the remaining three hydrogens are located below the x–y-plane. In each of the four minima of the whole $CH_4 \cdot F^-$ complex, the fluorine is collinear with the carbon and one of the four hydrogens. Thus, to be able to describe the minimum corresponding to the hydrogen that lies on the positive z-axis, the Jacobi vector associated with the fluorine has to be parametrized using stereographic coordinates that result from the south pole projection. Then, the s_F,t_F coordinates approximately correspond to the normal modes of this PES minimum. Consequently, the correlation between s_F and t_F is minimized, yielding a beneficial description of the dynamics. For the remaining three minima, these stereographic coordinates are less advantageous. With a given basis set size of the wave function representation, the local dynamics will thus

dx.doi.org/10.1021/jp3052642 | J. Phys. Chem. A XXXX, XXX, XXX–XXX

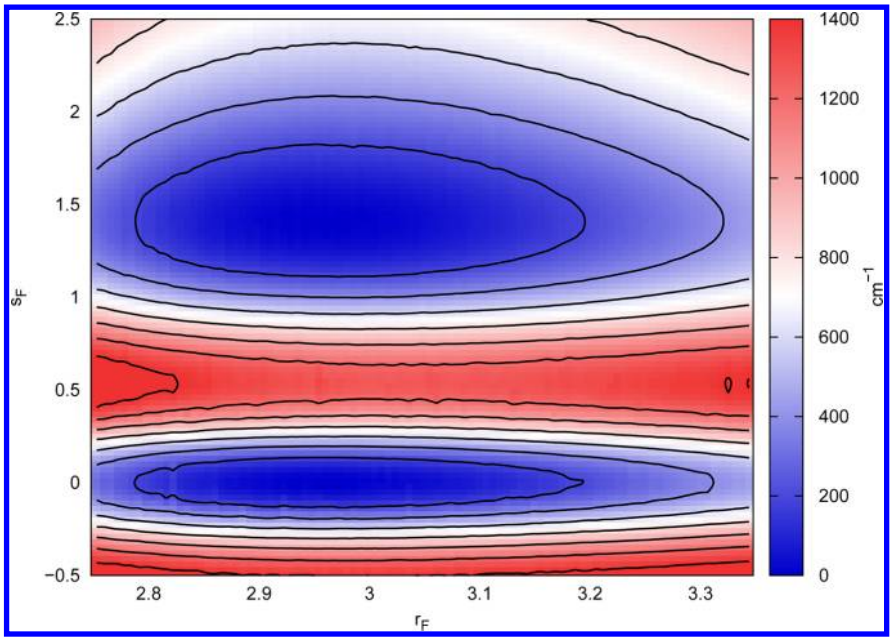

Figure 3. Contour plot of the $CH_4 \cdot F^-$ PES with respect to the coordinates r_F,s_F. r_F is given in Å (no mass-weighting).

be described most accurately in the first well (i.e., when the fluorine is placed on the positive z-axis).

B. Potential. All calculations presented in this work employ the PES developed by Czakó et al.[29] Figures 2 and 3 show this PES as a function of the coordinate pairs s_F,t_F and r_F,s_F with all other coordinates relaxed, respectively. In Figure 2, the four minima of the PES showing tetrahedral symmetry are nicely displayed. The minimum at $s_F = t_F = 0$ corresponds to the fluorine being located on the positive z-axis, while the remaining three minima correspond to the fluorine lying below the x−y-plane. The apparently unsymmetric "sizes" of the potential wells are a direct consequence of the properties of the stereographic coordinates employed. Though stereographic projection preserves angles (i.e., is conformal), it does not preserve lengths. Employing south pole projection, a given distance located in the southern hemisphere appears larger in the s,t space than the same distance located in the northern hemisphere. The contour plot employing the r_F,s_F coordinates shown in Figure 3 illustrates the transition-state region between two different potential wells. The potential barrier relative to the minimum is about 1270 cm^{-1}.

The harmonic frequencies with respect to one of the four potential minima[29] are given in Table 1. It is noteworthy that the intermolecular stretching mode (ν_s = 200 cm^{-1}) shows a lower frequency than the bending one (ν_b = 276 cm^{-1}). The ν_s mode corresponds to a $F^- - CH_4$ stretching motion. In contrast, the ν_b mode describes mainly rotations of the CH_4 around axes perpendicular to the line connecting F and C. Thus, the relative masses associated with each type of motion are quite different. In the stretching mode, the effective mass that undergoes the vibration is approximately given by the reduced mass of methane and fluorine. In the bending mode, the relevant moment of inertia is approximately given by the moment of inertia of CH_4 because the rotation of the fluorine is hindered by its large mass and the large distance of the fluorine from the center of mass of methane. Thus, while the heavy atoms C and F vibrate in the stretching mode, in the bending mode, only light H atoms rotate.

Table 1. Harmonic Frequencies of the $CH_4 \cdot F^-$ Complex in cm^{-1}[a]

mode	
$\nu_s(A_1)$	200
$\nu_b(E)$	276
$\nu_4(A_1)$	1296
$\nu_4(E)$	1395
$\nu_2(E)$	1570
$\nu_{hb}(A_1)$	2782
$\nu_3(A_1)$	3024
$\nu_3(E)$	3074

[a]Taken from ref 29.

The other nine vibrational coordinates correspond to intramolecular vibrations of the CH_4 and show significantly higher vibrational frequencies. Thus, their fundamental excitations are located in an energy range where the density of the vibrational states is already rather high due to the intermolecular motions. Thus, the present relaxation-based approach cannot address intramolecular vibrational excitations or corresponding resonances in the $CH_4 \cdot F^-$ complex.

C. Symmetry. The symmetry group of the nuclear Hamiltonian of the $CH_4 \cdot F^-$ complex is G_{48}. It is a direct product of S_4 (the permutation group of the four hydrogens) and the inversion group $I = \{E,E^*\}$, that is, $G_{48} = S_4 \otimes I$.[66,67] However, any symmetry transformation changing the chirality of the CH_4 core is hindered by an insuperable potential barrier. Consequently, half of the elements in G_{48} can be ignored, yielding a group isomorphic to the T_d point group. Thus, the irreducible representations of T_d can be used to label the global energy eigenstates.

Accounting for the physical significance of localized states, an alternative view offered by Altmann can be utilized.[68] There, the symmetry group G of a nonrigid molecule is written as a product of a so-called isodynamic group G_I connecting the energetically equivalent reference structures located at the minima of the potential and the point group G_R associated with the reference structures themselves, that is, $G = G_I \wedge G_R$, where

dx.doi.org/10.1021/jp3052642 | J. Phys. Chem. A XXXX, XXX, XXX−XXX

the product is written in its general, semidirect form. The $CH_4{\cdot}F^-$ complex exhibits four such isoenergetic structures because the potential has four equivalent minima corresponding to the four possible C_{3v}-symmetric $F^-{-}H{-}CH_3$ structures. Labeling the hydrogens from 1 to 4, the transformation among the structures can be realized by the operations of the group $G_I = V_4 = \{E, (12)(34), (13)(24), (14)(23)\}$, which is a normal divisor of S_4 and isomorphic to the point groups C_{2v} and D_2. One particular reference structure, on the other hand, exhibits C_{3v} point group symmetry, that is, $G_R = C_{3v}$. For the reference structure associated with the first hydrogen, for instance, the point group elements read $G_R = \{E, (12)^*, (13)^*, (23)^*, (123), (132)\}$ (please note that $(12)^* = E^*(12) = (12)E^*$). The overall symmetry is obtained from the semidirect product $G = V_4 \wedge C_{3v} = T_d$, consistent with the considerations above.

Because the four minima present in the $CH_4{\cdot}F^-$ complex are equivalent, the respective localized vibrational states obtained from eq 17 should be equal for each well. Due to the coordinates employed, only the hydrogens described by the stereographic coordinates are treated on the same footing. Thus, results for the localized vibrational states obtained from numerical calculations will differ between the wells if the calculations are not perfectly converged. This may be an issue if the coupling between the wells is rather weak, resulting in small splittings in the spectrum of the global states. Then, the errors introduced by the artificial differences in the local states might exceed the splittings, leading to misinterpretations. This could be, in principle, avoided by applying the operations of the group V_4 to the wave functions localized in the first well, for instance, to obtain the functions in the remaining three wells, as was done in ref 46. However, the coordinate system used in the present work does not allow for a straightforward transformation of the wave functions, especially with regard to the conservation of the MCTDH structure of linear combinations of Hartree products (see eq 10). The direct transformation of wave functions can be avoided if symmetry is introduced only when solving the generalized eigenvalue problems of eqs 16 and 17. To this end, the substitution (see eq 17 for the definition of the $\tilde{\epsilon}_{w,m}$)

$$\tilde{\epsilon}_{w,m} = \langle \psi^{(lok)}_{w,m} | e^{-i\hat{H}t} | \psi^{(lok)}_{w,m} \rangle = \langle \psi^{(lok)}_{1,m} | e^{-i\hat{H}t} | \psi^{(lok)}_{1,m} \rangle = \tilde{\epsilon}_{1,m}$$
$$m = 1, ..., P{\cdot}n; \quad w = 2, ..., W \tag{19}$$

can be made to enforce all of the local eigenvalues to be equal to the ones in the first well (which will be described most accurately as discussed in section 3A). The new ("symmetrized") matrices of the local representation of the operator $\exp(-i\hat{H}t)$ can now be obtained by back-transforming eq 18, that is

$$\langle e^{-\beta\hat{H}} \psi^{(i)}_{wp} | e^{-i\hat{H}t} | e^{-\beta\hat{H}} \psi^{(j)}_{wq} \rangle$$
$$= \sum_{k,l=1}^{P{\cdot}n} (\tilde{c}^{-1})^{(i)*}_{k,wp} (\tilde{c}^{-1})^{(j)}_{l,wq} \langle \psi^{(lok)}_{w,k} | e^{-i\hat{H}t} | \psi^{(lok)}_{w,l} \rangle$$
$$= \sum_{k=1}^{P{\cdot}n} (\tilde{c}^{-1})^{(i)*}_{k,wp} (\tilde{c}^{-1})^{(j)}_{k,wq} \tilde{\epsilon}_{1,k} \tag{20}$$

The values of these local matrices then replace the matrix elements diagonal in the well index (i.e., $w = v$) of the global representation of $\exp(-i\hat{H}t)$ in eq 16. Consequently, solving this modified global generalized eigenvalue problem, the differences between the local and global energies now result only from the coupling between different wells.

D. Wave Function Representation. The multilayer MCTDH wave function representation employed in all dynamical calculations is shown diagrammatically in Figure 4.

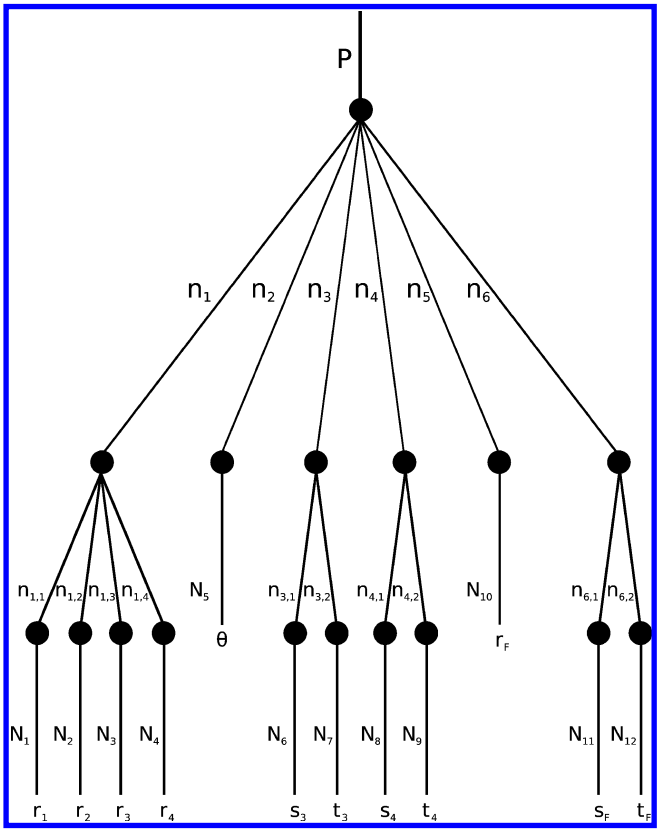

Figure 4. Diagrammatic representation of the multilayer MCTDH wave function.

Each solid circle represents one set of expansion coefficients $\boldsymbol{A}$ (see eqs 10−12). The label beside each line that connects two circles denotes the size of the corresponding SPF basis set ϕ employed. P is the number of state-averaged MCTDH wave packets used. The $\{N_i, i = 1, ..., 12\}$ indicate the sizes of the time-independent grids (see ref 58 for a more detailed explanation of the diagrammatic representation).

Harmonic oscillator DVR schemes are used to represent the SPFs in the coordinates $\{r_i, i = 1, ..., 4\}$ (32 grid points per coordinate) and r_F (120 grid points). SPF basis functions in the coordinate θ employ a Legendre DVR with 40 grid points. In the block relaxation calculations, FFT schemes with 48 grid points per coordinate are used to represent all functions in the stereographic coordinates. Here, only initial guess functions that are located in the first well are employed (see the discussion in section 3A). Thus, the grids in s_F and t_F are constructed to describe the dynamics appropriately only in this region. In the iterative diagonalization approach, the grids used for the functions in the fluorine coordinates s_F,t_F are enlarged to 144 points per coordinate. Here, all wells have to be described simultaneously (see section 2C). Consequently, the grids in s_F and t_F have to be enlarged to make all wells dynamically accessible.

The SPF basis set sizes employed in the block relaxation and iterative diagonalization calculations are given in Table 2. All

dx.doi.org/10.1021/jp3052642 | J. Phys. Chem. A XXXX, XXX, XXX−XXX

Table 2. Wave Function Representations Employed in the Block Relaxation and Iterative Diagonalization Calculations

	SPF basis			
	B1	B2	B3	B4
n_1	6	8	10	6
n_2	4	5	6	4
n_3	12	14	16	12
n_4	12	14	16	12
n_5	3	4	5	5
n_6	11	13	15	15
$n_{1,1}$	2	3	4	2
$n_{1,2}$	2	3	4	2
$n_{1,3}$	2	3	4	2
$n_{1,4}$	2	3	4	2
$n_{3,1}$	4	5	6	4
$n_{3,2}$	5	6	7	5
$n_{4,1}$	4	5	6	4
$n_{4,2}$	5	6	7	5
$n_{6,1}$	4	5	6	6
$n_{6,2}$	4	5	6	6

calculations employ four wave packets in the state-averaged MCTDH approach, that is, $P = 4$, and an imaginary propagation time of $\beta = 300$ au in the iteration step. In the multiwell iterative diagonalization, a time period of $t = 100$ au is used in the real time propagation step. Converged results could be obtained within 16 Lanczos iterations.

4. RESULTS

A. Block Relaxation Calculations. As a first step, reference results for the four lowest vibrational states localized in a single potential well were obtained by employing the block relaxation of state-averaged MCTDH wave functions.[52] Propagating the set of localized initial wave functions in imaginary time, no tendency of delocalization into the other potential wells was obtained. This observation indicates that the coupling between the different potential wells is weak.

To allow for a detailed analysis of the accuracy achieved, three different basis sets of systematically increasing size, denoted B1, B2, and B3, are employed. The numbers of SPFs used in these basis sets is given in Table 2. Stepping from B1 to B2 and then to B3, in each step, the number of SPFs in all physical coordinates is increased by one and that in all logical coordinates, that is, combined modes, by two. The calculated energy levels are given in Table 3.

Considering first the zero-point energy (denoted ν_0 in the table), energy differences of 3.5 and 1.1 cm^{-1} are found when increasing the basis set size from B1 to B2 and from B2 to B3, respectively. Thus, it is reasonable to expect that the value of 9786.6 cm^{-1} obtained with the largest basis set is converged to about 1 cm^{-1} accuracy. Even higher accuracies are achieved for the excitation energies. The corresponding energy differences for the stretching mode ν_s read 0.4 and 0.1 cm^{-1}, clearly indicating subwavenumber accuracy. Because the numerical methods employed do not impose the local C_{3v} symmetry by construction, two different energy values are computed for the excitation in the degenerate bending mode ν_b. This difference only vanishes in the limit of a converged SPF basis. Analyzing again the convergence behavior displayed in Table 3, it seems reasonable to expect that the excitation energy of 268 cm^{-1} obtained with basis set B3 is converged to an accuracy of at least one cm^{-1}. It should be noted that this convergence study simultaneously addresses the issues of wave function representation and potential quadrature because the number of quadrature points employed in the CDVR quadrature simultaneously increases with the size of the SPF basis employed.

Table 3. Local Ground-State Energy and Local Vibrational Excitation Energies of the First Three Excited States in cm^{-1} Calculated Employing the Block Relaxation Approach[a]

	SPF basis			
level	B1	B2	B3	ref 29
$\nu_0(A_1)$	9791.2	9787.7	9786.6	9794.7
$\nu_s(A_1)$	193.8	193.4	193.3	201.1
$\nu_b(E)$	271.3	268.8	268.1	299.9
	272.1	269.2	268.4	299.9

[a]The corresponding energy values from ref 29 are shown for comparison.

Czakó et al.[29] investigated the local vibrational states of the $CH_4 \cdot F^-$ complex on the same potential surface. Their calculations employed normal coordinates and a VCI[30] approach that utilizes an n-mode representation of the potential and an excitation-class-based truncation scheme to reduce the CI space (see ref 31 for a detailed description). Their results, which differ significantly from our present ones, are also given in Table 3. The comparison with the harmonic frequencies given in Table 1 highlights the differences between our results and the ones of Czakó et al. While the present results indicate that the F−CH_4 stretching excitation energy is reduced from the harmonic value of 200 to 193 cm^{-1} due to anharmonicity, Czakó et al. obtained an excitation energy slightly above the harmonic value. Considering the intermolecular bending, the present calculations yield a decrease from 276 to 268 cm^{-1} due to anharmonicity. In contrast, Czakó et al. find a significant increase to 299.9 cm^{-1}.

The disagreement between our present results and the ones of Czakó et al. is surprising because, like the MCTDH approach, the VCI approach in principle is a numerically exact method. Errors can only result from incomplete convergence of the (truncated) basis sets representations or the potential quadrature. Considering our MCTDH calculations, we think that the convergence study presented above convincingly establishes the accuracy of the present MCTDH results. Considering the VCI calculations, three potential sources of errors are listed in the work of Czakó et al., the number of simultaneous excitations in different modes considered in the truncated VCI expansions, the number of excitation quanta considered for each mode, and the number of modes simultaneously considered in the n-mode representation of the potential. A convergence study addressing all of the issues was presented by Czakó et al., but the maximum number of configurations included in their VCI calculations was rather limited; it included a maximum of 21 348 configurations. In contrast, the basis sets B1, B2, and B3 used in the present MCTDH calculation employ 114 048, 407 680, and 1 152 000 configurations, respectively, for each of the four vibrational states considered. In addition, the maximum number of modes that could be simultaneously excited was limited to five in the VCI calculation. Thus, we assume that the use of normal coordinates to describe the large-amplitude intermolecular motion in the $CH_4 \cdot F^-$ complex resulted in artificially slow convergence in the truncated VCI scheme. This could not be

dx.doi.org/10.1021/jp3052642 | J. Phys. Chem. A XXXX, XXX, XXX−XXX

detected in the convergence test due to the limitations in the configuration space considered. Considering that the MCTDH and VCI approaches are, in principle, variational (except for the errors due to the potential quadrature employed), the fact that the present vibrational energies are always lower than VCI ones also supports this assumption.

B. Multiwell Iterative Diagonalization. As in the block relaxation calculations, the multiwell iterative diagonalization calculations employed the basis sets B1, B2, and B3. While results converged with respect to the number of iterations could be obtained for basis sets B1 and B2, the basis B3 has been numerically too demanding to perform many Lanczos iterations. For this base, only three Lanczos iterations could be computed, and the results are reasonably well converged with respect to the number of iterations only for the local ground state and the corresponding tunneling splittings. To investigate the convergence of the locally excited vibrational states, the additional basis set B4 (see Table 2) is utilized. This basis employs the same SPF basis sizes in the intermolecular modes as B3 but restricts the number of SPFs in the intramolecular modes to the values taken in B1. Comparing the basis B2 and B4, B2 includes more SPFs in the intramolecular modes, while B4 uses more SPFs in the intermolecular ones. The total numerical effort for calculations with the basis B2 and B4 is roughly comparable, and thus, convergence with respect to the number of iterations could also be achieved for the basis B4. As a basis for the investigation of the delocalized vibrational states by the multiwell iterative diagonalization approach, first, the local states obtained by eq 17 are studied. The computed energies of the vibrational states localized in the first well are presented in Table 4. Considering the zero-point energy ν_0 and the first two fundamentals ν_s and ν_b computed with the basis B1 and B2, the results obtained by iterative diagonalization are quite similar to the ones computed with the same basis sets by block relaxation (see Table 3). Thus, the accuracy achieved with the iterative diagonalization approach seems to be comparable with the accuracy of the block relaxation results obtained with the same SPF basis. Comparing the results obtained with the different basis sets and considering the energy differences of states that theoretically should be degenerate, one can estimate that the results obtained with the larger basis sets are converged to within a few cm^{-1}. The excitation energies for the fundamental and the first overtone of the stretching mode are presumably converged within wavenumber accuracy, but larger uncertainties are found for the bending overtones and the combined stretching and bending excitation. Here, the differences between the results obtained with the larger basis sets B2 and B4 increase up to 2.5 cm^{-1}. For the combined stretching and bending excitation, even a 5 cm^{-1} difference for the excitation into the two components of this degenerate level is found using the B2 basis. The B4 basis yields more reliable results for this excitation; here, the difference is less than 1 cm^{-1}.

Table 4. Local Ground-State Energy and Local Vibrational Excitation Energies of the First Nine Excited States in cm^{-1} Calculated in the First Well Employing the Multiwell Iterative Diagonalization Approach

	SPF basis			
local vibrational excitation	B1	B2	B3	B4
$\nu_0(A_1)$	9791.5	9787.7	9787.0	9791.2
$\nu_s(A_1)$	193.6	193.2		193.6
$\nu_b(E)$	271.1	269.1		270.8
	272.3	269.7		271.5
$[2\nu_s](A_1)$	386.8	379.1		379.7
$[\nu_s + \nu_b](E)$	462.0	457.1		459.5
	463.7	462.4		460.6
$[2\nu_b](A_1)$	542.6	525.5		528.0
$[2\nu_b](E)$	551.5	546.4		544.9
	567.8	548.8		546.9

Studying the convergence behavior in more detail, a comparison between the B2 and B4 results is particularly interesting. One would naively expect that the B4 basis, which uses the largest number of SPFs in the intermolecular coordinates, should yield the most accurate results for the excitation energies of the intermolecular modes. However, the B2 basis clearly yields more accurate results for the excitation energy in the bending fundamental. This finding indicates that the intermolecular and intramolecular modes are rather strongly correlated. Finally, the delocalized vibrational eigenstates of the $CH_4{\cdot}F^-$ complex are investigated. These rigorous eigenstates (for vanishing total angular momentum $J = 0$) are calculated by the multiwell iterative diagonalization approach using eq 16 and symmetrized matrix elements obtained as described in section 3C. The resulting energies are given in Table 5.

The ground-state tunneling splitting is particularly interesting because it could affect the photodetachment spectrum observed in experiment. Theoretically, the delocalization between the four wells splits the four local vibrational ν_0 states into the global vibrational ground state, which transforms according to the A_1 irreducible representation of the T_d group, and the triply degenerated $1F_2$ state. Comparing the results obtained with the different basis sets, one cannot reliably obtain an accurate value for the tunneling splitting between the global $1A_1$ ground state and the $1F_1$ level. While a still sizable splitting of about 3 cm^{-1} is computed with the small B1 basis, this splitting decreases to about 1 cm^{-1} and below for all larger basis. Thus, one can reliably conclude that the ground-state tunneling splitting does not significantly exceed 1 cm^{-1} and thereby establish an upper boundary of about 1 cm^{-1} for the tunneling splitting. However, given the presently available data, one should not attempt to provide a lower boundary for the accurate value of the tunneling splitting.

The results of Table 5 clearly show that the tunneling splittings of the local vibrational excited states are similarly small. Considering locally excited states of A_1 symmetry, the tunneling splittings obtained with the larger basis sets B2 and B4 are always below 1 cm^{-1}. For the locally excited states of E symmetry, one has to note that already, the two different components of the local representation are not perfectly degenerate (see Table 4). Here, the additional splittings introduced by the interwell interaction are again always below 1 cm^{-1}.

In conclusion, the present results clearly demonstrate that the tunneling splittings in the $CH_4{\cdot}F^-$ complex do not exceed about 1 cm^{-1} for vibrational states that could be thermally populated under experimental conditions. Considering the simulation and theoretical analysis of the high-resolution $CH_4{\cdot}F^-$ photodetachment spectrum, this upper boundary is sufficiently low to establish that the delocalization of the $CH_4{\cdot}F^-$ complex can be safely disregarded in the description.

dx.doi.org/10.1021/jp3052642 | J. Phys. Chem. A XXXX, XXX, XXX−XXX

Table 5. Global Ground-State Energy and Global Vibrational Excitation Energies of the First 39 Excited States in cm^{-1} Calculated Employing the Multiwell Iterative Diagonalization Approach

	SPF basis			
local vibrational excitation	B1	B2	B3	B4
ν_0	9788.3	9786.5	9786.5	9790.3
	3.2	0.8	0.4	0.6
	3.2	1.0	0.5	0.8
	3.4	1.2	0.5	0.9
ν_s	196.5	194.3		194.4
	196.8	194.4		194.4
	196.8	194.4		194.5
	196.9	194.5		194.5
ν_b	274.2	270.1		271.7
	274.3	270.1		271.7
	274.3	270.3		271.7
	274.5	270.4		271.8
	274.8	270.4		271.9
	275.4	270.9		272.4
	275.6	271.2		272.5
	275.8	271.2		272.8
$[2\nu_s]$	390.0	380.3		380.6
	390.0	380.3		380.7
	390.0	380.3		380.7
	390.0	380.4		380.7
$[\nu_s + \nu_b]$	465.1	458.3		460.2
	465.2	458.3		460.3
	465.2	458.3		460.4
	465.2	458.3		460.4
	466.5	463.6		461.4
	466.6	463.6		461.5
	466.6	463.6		461.5
	466.6	463.6		461.5
$[2\nu_b]$	541.7	526.6		528.7
	545.5	526.7		528.9
	545.5	526.7		528.9
	548.9	526.7		529.1
$[2\nu_b]$	554.7	547.3		545.7
	554.7	547.4		545.8
	554.7	547.5		545.8
	554.7	547.6		545.8
	571.0	550.0		547.7
	571.0	550.0		547.8
	571.0	550.0		547.8
	571.0	550.3		547.8

5. CONCLUSIONS

A detailed investigation of the vibrational states of the $CH_4 \cdot F^-$ complex focusing on the intermolecular modes was presented. Accurate full-dimensional calculations of the vibrational eigenstates have been performed using the state-averaged multilayer MCTDH/CDVR approach. While localized vibrational states could be computed via the well-established block relaxation scheme, a recently developed iterative diagonalization approach for multiwell system has been employed to study the tunneling splittings resulting from delocalization.

To adequately describe the large-amplitude motion in the intermolecular modes, a curvilinear coordinate system has been used. This coordinate system uses stereographic coordinates to parametrize Jacobi and Radau vectors. Extending earlier work on stereographic coordinates, a generalized definition that employs either north or south pole projection is presented. A corresponding general *N*-body kinetic energy operator that can be applied to a wide range of systems is derived.

The tunneling splittings resulting from delocalization via the four symmetry-equivalent wells in the $CH_4 \cdot F^-$ PES are found to be small. They do not significantly exceed 1 cm^{-1} for the ground state or the vibrationally excited states with excitation energies below 550 cm^{-1}. Thus, delocalization of the vibrational eigenstates of $CH_4 \cdot F^-$ will not significantly affect even high-resolution photodetachment spectra. There the resonance structures that show spacings in the 10−30 cm^{-1} range.[25] Localized initial wave packets can thus reliably be employed in quantum dynamics simulations of $CH_4 \cdot F^-$ photodetachment.

Considering vibrational excitation in the intermolecular stretching and bending modes, surprisingly large differences between the present results and the VCI results of Czakó et al.[29] have been found. They are particularly large for the bending mode that mainly corresponds to a rotation of the methane molecule relative to the F−C axis. Here, the combined use of rectilinear normal modes, which can not describe large-amplitude rotational type motion in the separable (VSCF) picture, and an aggressively truncated VCI expansion seems to produce errors due to incomplete convergence that cannot easily be monitored even by rather careful convergence tests.

AUTHOR INFORMATION

Corresponding Author

*E-mail: uwe.manthe@uni-bielefeld.de.

Notes

The authors declare no competing financial interest.

†E-mail: robert.wodraszka@uni-bielefeld.de (R.W.); juliana@unq.edu.ar (J.P.).

ACKNOWLEDGMENTS

We thank to Gabor Czakó and Joel Bowman for providing us with the potential energy surface code. Financial support by the Deutsche Forschungsgemeinschaft is gratefully acknowledged. J.P. is very grateful to the Alexander von Humboldt foundation and the Consejo Nacional de Investigaciones Científicas y Técnicas (CONICET) for financial support.

REFERENCES

(1) Harper, W. W.; Nizkorodov, S. A.; Nesbitt, D. J. *J. Chem. Phys.* **2000**, *113*, 3670.
(2) Lin, J.; Zhou, J.; Shiu, W.; Liu, K. *Science* **2003**, *300*, 966.
(3) Shiu, W.; Lin, J.; Liu, K. *Phys. Rev. Lett.* **2004**, *92*, 103201.
(4) Zhang, W.; Kawamata, H.; Liu, K. *Science* **2009**, *325*, 303.
(5) Czakó, G.; Shuai, Q.; Liu, K.; Bowman, J. M. *J. Chem. Phys.* **2010**, *133*, 131101.
(6) Czakó, G.; Shepler, B. C.; Braams, B. J.; Bowman, J. M. *J. Chem. Phys.* **2009**, *130*, 084301.
(7) Czakó, G.; Bowman, J. M. *Phys. Chem. Chem. Phys.* **2011**, *13*, 8306.
(8) Kim, Z. H.; Bechtel, H. A.; Zare, R. N. *J. Am. Chem. Soc.* **2001**, *123*, 12714.
(9) Yoon, S.; Henton, S.; Zivkovic, A. N.; Crim, F. F. *J. Chem. Phys.* **2002**, *116*, 10744.
(10) Retail, B.; Pearce, J. K.; Murray, C.; Orr-Ewing, A. J. *J. Chem. Phys.* **2005**, *122*, 101101.
(11) Yan, S.; Wu, Y.-T.; Zhang, B.; Yue, X.-F.; Liu, K. *Science* **2007**, *316*, 1723.
(12) Yan, S.; Wu, Y.-T.; Zhang, B.; Yue, X.-F.; Liu, K. *Proc. Natl. Acad. Sci. U.S.A.* **2008**, *105*, 12667.
(13) Yu, H.-G.; Nyman, G. *J. Chem. Phys.* **1999**, *110*, 7233.

(14) Rudic, S.; Mauuray, C.; Harvey, J. N.; Orr-Ewing, A. J. *J. Chem. Phys.* **2004**, *120*, 186.
(15) Yu, H.-G.; Nyman, G. *J. Chem. Phys.* **1999**, *111*, 3508.
(16) Wang, M.; Li, Y.; Zhang, J.; Zhang, D. *J. Chem. Phys.* **2000**, *113*, 1802.
(17) Huarte-Larrañaga, F.; Manthe, U. *J. Chem. Phys.* **2000**, *113*, 5115.
(18) Wu, T.; Werner, H.-J.; Manthe, U. *Science* **2004**, *306*, 2227.
(19) Zhang, W.; Zhou, Y.; Wu, G.; Lu, Y.; Pan, H.; Fu, B.; Shuai, Q.; Liu, L.; Liu, S.; Zhang, L.; et al. *Proc. Natl. Acad. Sci. U.S.A.* **2010**, *107*, 12782.
(20) Zhou, Y.; Wang, C.; Zhang, D. H. *J. Chem. Phys.* **2011**, *135*, 024313.
(21) Schiffel, G.; Manthe, U. *J. Chem. Phys.* **2010**, *132*, 191101.
(22) Schiffel, G.; Manthe, U. *J. Chem. Phys.* **2010**, *133*, 174124.
(23) Huarte-Larrañaga, F.; Manthe, U. *J. Chem. Phys.* **2002**, *117*, 4635.
(24) Cheng, M.; Feng, Y.; Du, Y.; Zhu, Q.; Zheng, W.; Czakó, G.; Bowman, J. M. *J. Chem. Phys.* **2011**, *134*, 191102.
(25) Yacovitch, T. I.; Garand, E.; Kim, J. B.; Hock, C.; Theis, T.; Neumark, D. M. *Faraday Discuss.* **2012**, DOI: 10.1039/c2fd20011b.
(26) Palma, J.; Manthe, U. *J. Chem. Phys.* **2012**, in press.
(27) Meyer, H.-D.; Manthe, U.; Cederbaum, L. S. *Chem. Phys. Lett.* **1990**, *165*, 73.
(28) Manthe, U.; Meyer, H.-D.; Cederbaum, L. S. *J. Chem. Phys.* **1992**, *97*, 3199.
(29) Czakó, G.; Braams, B. J.; Bowman, J. M. *J. Phys. Chem. A* **2008**, *112*, 7466.
(30) Bowman, J. M.; Christoffel, K.; Tobin, F. *J. Phys. Chem.* **1979**, *83*, 905.
(31) Bowman, J. M.; Carter, S.; Huang, X. *Int. Rev. Phys. Chem.* **2003**, *22*, 533.
(32) Yu, H.-G. *J. Chem. Phys.* **2004**, *120*, 2270.
(33) Wang, X.-G.; Carrington, T., Jr. *J. Chem. Phys.* **2008**, *129*, 234102.
(34) Vendrell, O.; Gatti, F.; Lauvergnat, D.; Meyer, H.-D. *Angew. Chem., Int. Ed.* **2007**, *46*, 6918.
(35) Vendrell, O.; Gatti, F.; Lauvergnat, D.; Meyer, H.-D. *J. Chem. Phys.* **2007**, *127*, 184302.
(36) Vendrell, O.; Gatti, F.; Meyer, H.-D. *J. Chem. Phys.* **2007**, *127*, 184303.
(37) Vendrell, O.; Brill, M.; Gatti, F.; Meyer, H.-D. *J. Chem. Phys.* **2009**, *130*, 234305.
(38) Vendrell, O.; Gatti, F.; Meyer, H.-D. *J. Chem. Phys.* **2009**, *131*, 034308.
(39) Coutinho-Neto, M. D.; Viel, A.; Manthe, U. *J. Chem. Phys.* **2004**, *121*, 9207.
(40) Viel, A.; Coutinho-Neto, M. D.; Manthe, U. *J. Chem. Phys.* **2007**, *126*, 024308.
(41) Hammer, T.; Coutinho-Neto, M. D.; Viel, A.; Manthe, U. *J. Chem. Phys.* **2009**, *131*, 224109.
(42) Wang, Y.; Braams, B. J.; Bowman, J. M.; Carter, S.; Tew, D. P. *J. Chem. Phys.* **2008**, *128*, 224314.
(43) Hammer, T.; Manthe, U. *J. Chem. Phys.* **2011**, *134*, 224305.
(44) Schroeder, M.; Gatti, F.; Meyer, H.-D. *J. Chem. Phys.* **2011**, *134*, 234307.
(45) Hammer, T.; Manthe, U. *J. Chem. Phys.* **2012**, *136*, 054105.
(46) Wodraszka, R.; Manthe, U. *J. Chem. Phys.* **2012**, *136*, 124119.
(47) Schiffel, G.; Manthe, U. *J. Chem. Phys.* **2010c**, *132*, 084103.
(48) Wang, X.-G.; Carrington, T., Jr. *J. Chem. Phys.* **2000**, *113*, 7097.
(49) Tennyson, J.; Sutcliffe, B. T. *J. Chem. Phys.* **1982**, *77*, 4061.
(50) Zare, R. N. *Angular Momentum*; Wiley: New York, 1988.
(51) Meyer, H.-D.; Gatti, F.; Worth, G. A. *Multidimensional Quantum Dynamics: MCTDH Theory and Applications*; Wiley-VCH: Weinheim, Germany, 2009.
(52) Manthe, U. *J. Chem. Phys.* **2008**, *128*, 064108.
(53) Harris, D. O.; Engerholm, G. G.; Gwinn, W. D. *J. Chem. Phys.* **1965**, *43*, 1515.
(54) Dickinson, A. S.; Certain, P. R. *J. Chem. Phys.* **1968**, *49*, 4209.
(55) Light, J. C.; Hamilton, I. P.; Lill, J. V. *J. Chem. Phys.* **1985**, *82*, 1400.
(56) Kosloff, D.; Kosloff, R. *J. Comput. Phys.* **1983**, *52*, 35.
(57) Wang, H.; Thoss, M. *J. Chem. Phys.* **2003**, *119*, 1289.
(58) Manthe, U. *J. Chem. Phys.* **2008**, *128*, 164116.
(59) Beck, M. H.; Meyer, H.-D. *Z. Phys. D* **1997**, *42*, 113.
(60) Manthe, U. *Chem. Phys.* **2006**, *329*, 168.
(61) Manthe, U. *J. Chem. Phys.* **1996**, *105*, 6989.
(62) van Harrevelt, R.; Manthe, U. *J. Chem. Phys.* **2005**, *123*, 064106.
(63) Manthe, U. *J. Chem. Phys.* **2009**, *130*, 054109.
(64) Manthe, U.; Matzkies, F. *Chem. Phys. Lett.* **1996**, *252*, 71.
(65) Meyer, H.-D.; Quere, F. L.; Leonard, C.; Gatti, F. *Chem. Phys.* **2006**, *329*, 179.
(66) Longuet-Higgins, H. C. *Mol. Phys.* **2002**, *100*, 11.
(67) Bunker, P. R.; Jensen, P. *Molecular Symmetry and Spectroscopy*; NRC Research: Ottawa, Canada, 1998.
(68) Altmann, S. L. *Proc. R. Soc. London, Ser. A* **1967**, *298*, 184.